MODELING AND ANALYSIS OF A DC ELECTROSTATIC VIBRATION-TO-ELECTRICITY MICRO POWER GENERATOR

Yi Chiu*, Ching-Fu Chang
Department of Electrical Engineering, National Chiao Tung University, Hsin Chu, Taiwan, R.O.C.
*Presenting Author: yichiu@mail.nctu.edu.tw

Abstract: This paper presents the analytical modeling of the nonlinear dynamics of a DC battery-charged vibration-to-electricity energy converter. Prior design of such converters relied on simplified linear modeling or time-domain simulation. The electromechanical dynamics of the conversion was thus over-simplified or overlooked. In this paper, an equation-based modeling methodology is presented. Optimal design and maximum output power are obtained by solving the nonlinear equations of motion. It is found that optimized converters can generate significant power only for a limited range of design and operation parameters. Over certain range of parameters, the converters can not operate stably.

Keywords: energy harvesting, electrostatic, vibration, nonlinear dynamics, equation of motion

1. INTRODUCTION

Low power CMOS VLSI technology has enabled the development of applications such as wireless sensor networks or personal health monitoring. In these applications, lifetime and maintenance of the power supply is critical. Recently, energy scavenging from ambient natural sources, such as vibration and ambient heat, is attracting much interest as self-sustainable power sources. Among various approaches, electrostatic vibration-to-electricity conversion is promising due to its compatibility to IC processes and the ubiquity of vibration source in nature.

Electrostatic vibration-to-electricity micro power generators can be charged by an auxiliary power supply and operated in DC mode [1]. Prior design of such generators relied on simplified linear modeling [1] or time-domain simulation [2-5]. The nonlinear electromechanical dynamics of the energy conversion cycles was thus over-simplified or overlooked. In this paper, an equation-based modeling methodology is presented. Exact solutions of the system are obtained by solving the nonlinear equations of motion for a given set of design and operation parameters. Optimal design and maximum output power can thus be found by searching a range of these parameters.

Since the output power of a vibration-driven converter is related to the characteristics of the vibration source, a typical vibration of 2.25 m/s^2 at about 120 Hz, found in a number of household appliances, is used as the energy source for the design of the optimal generator in this paper.

2. PRINCIPLE AND ANALYSIS

The operation of the DC converter is shown in Figure 1 [1]. The circuit is composed of an auxiliary power supply V_{in} such as a battery, a vibration-driven variable capacitor C_v and an output storage capacitor C_{stor} connected with the load R_L. C_v is charged by V_{in} through SW1 at its maximum C_{max}, and discharged to C_{stor} through SW2 at its minimum C_{min} when the terminal voltage is at its maximum V_{max}. Mechanical energy is converted into electric energy through the increase of voltage of the constant charge on the variable capacitor. To achieve high conversion efficiency, the charge-discharge cycles must be timed precisely by SW1 and SW2 with the change of the capacitance.

The variable capacitor design for matching the vibration source and load resistance is related to the coupling of mechanical and electrostatic forces. In steady of simulation or linear approximation, an equation-based modeling is proposed in order to solve the system dynamics analytically. In the design flow, static analysis is first conducted to obtain guidelines for the overall parameters of the converter, including the output power and the load. The geometrical design of the variable capacitor is directly related to the seismic mass. Finally, dynamic analysis is conducted to determine the amplitude of the shuttle mass under the electrostatic coupling. The overall system optimization can be found by searching a range of these parameters.

2.1 Analysis

In the charge-discharge cycles, C_v has a constant charge Q_{max} and Q_{min} after charging and discharging, respectively. The charge ratio Q_r is defined as the ratio of the charges on the variable capacitor,

$$Q_r = Q_{min} / Q_{max} . \quad (1)$$

The voltage on the variable capacitor changes from

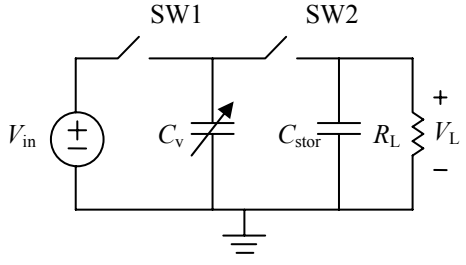

Fig. 1: Operation of the electrostatic energy converter.

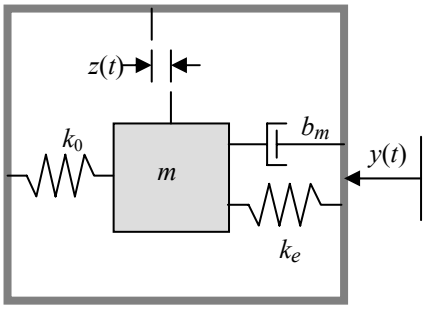

Fig. 2: Schematic of the conversion dynamic model.

V_{max} to V_o instantaneously when SW2 is closed at C_{min}. The output voltage V_o can be found from the charge balance between C_{min} and C_{stor} after they are connected by SW2. V_{max} and V_o are related by $V_o = Q_r V_{max}$. As a result, the load and the output power can be expressed by

$$R_L = \frac{Q_r}{2fC_{min}(1-Q_r)}, \tag{2}$$

$$P_{out} = 2fC_{min}V_{max}^2 Q_r(1-Q_r), \tag{3}$$

where the f is the vibration frequency. Therefore, Q_r can be used as a unique parameter to describe the performance characteristics in the design optimization.

In the dynamic modeling as shown in Figure 2, the equation of motion of the system can be written as

$$m\ddot{z}+b_m\dot{z}+(k_0+k_e)z=-m\ddot{y}, \tag{4}$$

where z is the displacement of the shuttle mass with respect to the device frame, y is the displacement of he device frame caused by the vibration, $b_m\dot{z}$ is the mechanical damping force. The electrostatic force $k_e z$ on the variable capacitor C_v with a constant charge Q is equivalent to a spring force with a negative spring constant k_e that is proportional to Q^2 [1]. Since Q alternates between Q_{max} and Q_{min} in steady conversion cycles, the total spring constant of the system is therefore a function of time,

$$k(t) = \begin{cases} k_1 = k_0 + k_{e,max}, & z(t)\dot{z}(t) < 0,\ Q = Q_{max} \\ k_2 = k_0 + k_{e,min}, & z(t)\dot{z}(t) > 0,\ Q = Q_{min} \end{cases}, \tag{5}$$

and the system is piecewise linear as expressed by

$$\begin{aligned} m\ddot{z}_1 + b_m\dot{z}_1 + k_1 z_1 &= -m\ddot{y},\ z(t)\dot{z}(t) < 0 \\ m\ddot{z}_2 + b_m\dot{z}_2 + k_2 z_2 &= -m\ddot{y},\ z(t)\dot{z}(t) > 0 \end{aligned}. \tag{6}$$

The variable capacitor with initial gap d has oscillation amplitude A when excited by the vibration, as shown in Figure 3. The difficulty in analyzing such a system is that the electrostatic spring constant k_e is

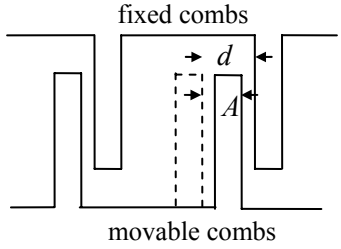

Fig. 3: The variable capacitor has initial gap d and oscillation amplitude A.

related to the oscillating amplitude A of the shuttle mass [1],

$$k_{e,max} = \frac{-2N\varepsilon L_f h d V_{in}^2}{(d^2 - A^2)^2}, \tag{7}$$

$$k_{e,min} = k_{e,max} Q_r^2. \tag{8}$$

Therefore both the system and its response are unknown before analysis. In previous analysis based on simulation software such as Simulink [5, 6], various values of system parameters, such as mass m and mechanical spring constant k_0, were tried in the simulation to find the best design. However, this approach is time-consuming and global optimization is difficult. In this paper, we demonstrate a new analytical modeling based on the equation of motion. System parameters such as k_e and system repsonse such as A are treated as unknowns in the analytical solution of the equation of motion. Numerical solutions can be applied to find these unknowns. Standard algorithms can also be applied to optimize the system expressed in analytical forms.

Since the equation of motion in Eq. 6 is a piecewise linear second-order differential equation, the two solutions z_1 and z_2 of the displacement function z can be written as the sum of general solutions and particular solutions [7],

$$\begin{aligned} z_1 &= e^{-\xi_1\omega_1 t}\left(C_1\cos\omega_{d1}t + C_2\sin\omega_{d1}t\right) + z_{p1}(t) \\ z_2 &= e^{-\xi_2\omega_2 t}\left(C_3\cos\omega_{d2}t + C_4\sin\omega_{d2}t\right) + z_{p2}(t) \end{aligned}, \tag{9}$$

where z_{p1} and z_{p2} are particular solutions .

Figure 4 is an illustration of the charge-discharge conversion cycles and oscillation of the shuttle mass. There are two identical conversion cycles in one

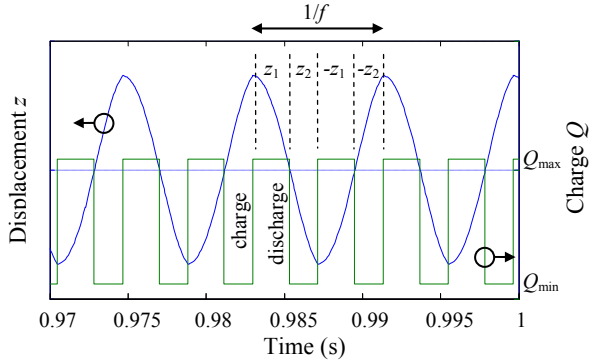

Fig. 4: Typical dynamic behavior of the shuttle mass.

vibration period; the second cycle is in the opposite direction with respect to the first one, as shown in Figure 4. To solve the piecewise linear equations, the time scale is set to start ($t = 0$) when the shuttle mass is at one of its maximum displacement. There is also a time delay ΔT between the excitation y and response z. For steady and smooth oscillation, certain boundary conditions must be met between z_1 and z_2 as shown below

$$\dot{z}_1(0) = 0\,,\ \dot{z}_2\left(\frac{1}{2f}\right) = 0\,, \tag{10}$$

$$z_1(0) = -z_2\left(\frac{1}{2f}\right),\ \left|z_1(0)\right| = A\,, \tag{11}$$

$$z_1\left(\frac{\alpha}{2f}\right) = 0\,,\ z_2\left(\frac{\alpha}{2f}\right) = 0\,, \tag{12}$$

$$\dot{z}_1\left(\frac{\alpha}{2f}\right) = \dot{z}_2\left(\frac{\alpha}{2f}\right), \tag{13}$$

where α is a parameter depicting unequal speeds during z_1 and z_2. In these boundary conditions, Eq. 10 means the velocity at both ends of displacement is equal to zero; Eq. 11 shows the amplitude at both ends is equal and its value is A; Eq. 12 shows that the displacement at center is zero; Eq. 13 is the continuity of velocity at center.

2.2 Calculation Results

Seven unknowns of the system dynamic response, namely C_1, C_2, C_3, C_4, α, ΔT, and A, can be solved from the above equations for a given set of device design and operation parameters. These parameters and their ranges for optimizing the converter for maximum output power is shown in Table 1 under a 1-cm^2 area constraint. S_r is the ratio of the capacitor area to the total chip area. It is positively related to the variable capacitance; however it should be limited for the robustness of the structure in actual design.

Because the equations are highly nonlinear, the nonlinear solver FSOLVE in Matlab was used to find the numerical solution. For small amplitude, the system can be approximated as linear. The solution of this linear system was used as the initial guess for the nonlinear solver. Once the numerical solution was found for the current set of optimization parameters, it could be used as the initial guess for the next set of parameter values. These steps were repeated until the entire range of the parameters was solved to find the optimized design.

Figure 5 shows an example of calculated amplitude and output power versus vibration frequency for a particular set of optimization parameters. It can be seen that the oscillation amplitude of the mass increases gradually as the frequency approaches the mechanical resonance. The output power increases with increasing amplitude so

Table 1: Optimization parameters and their range.

	Descriptions	Range
k_0	Mechanical spring constant	1 ~ 3000 N/m
Q_r	Charge ratio	0.1 ~ 0.9
S_r	Surface ratio	0.05 ~ 0.95
d	Finger initial gap	1 ~ 70 μm

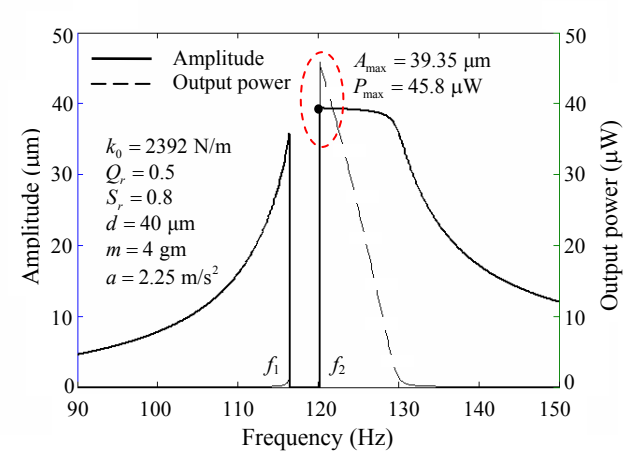

Fig. 5: Calculated amplitude and output power as a function of vibration frequency.

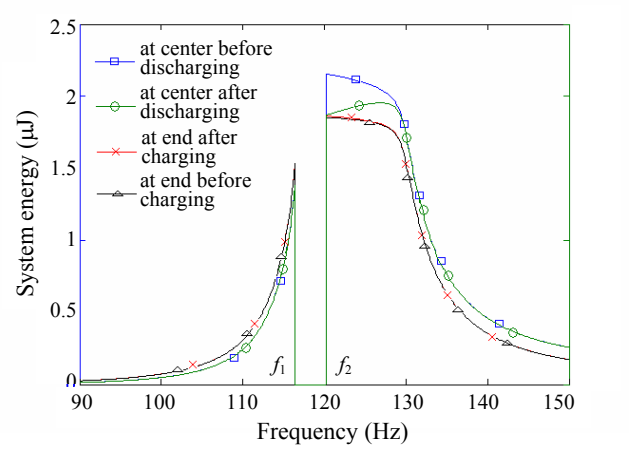

Fig. 6: System energy at four instants of oscillation.

that the system energy loss becomes larger near resonance. This limits the growing trend of the response between 120 and 130 Hz shown in Figure 5. As desired, the maximum amplitude and output power occurs at the targeted 120 Hz. However, Figure 5 also shows a range of frequency between f_1 and f_2 where numerical solutions could not be found, indicating no stable oscillation can be established in this range of frequency. The phenomenon can be explained from the viewpoint of system energy. Figure 6 shows the total system energy, including the kinetic energy, mechanical spring energy, and electrostatic capacitor energy, at different instants during oscillation. The output energy is the difference between the total energy at center before and after discharging. As the system approaches the resonance at f_2 with reducing frequency, the output reaches maximum and the

energy left in the system after discharging becomes equal to the energy of the system at maximum displacement. As the trend in Figure 6 shows, the system will not have enough energy to move from center to ends if the driving frequency is further reduced beyond f_2. Similar observation can be found at f_1 and therefore there is no stable oscillation in between.

3. OPTIMIZATION

From the above calculation, the output power can be maximized with respected to the initial capacitor gap d, area ratio S_r, and charge ratio Q_r over the range in Table 1. Figures 7 and 8 are contour plots of power and output voltage versus area ratio S_r and initial gap d with and without external mass. These figures correspond particularly to Q_r = 0.3 and Q_r = 0.6, respectively, for which the maximum power was found. Constant-voltage contours are represented by the thick lines in the plots. To allow the integration with power management circuits, the output voltage is limited to 40 V. Under these conditions, the maximum power is 38.1 μW and 0.87 μW for a device with and without a 4-gm external mass, respectively. The optimized design is summarized in Table 2.

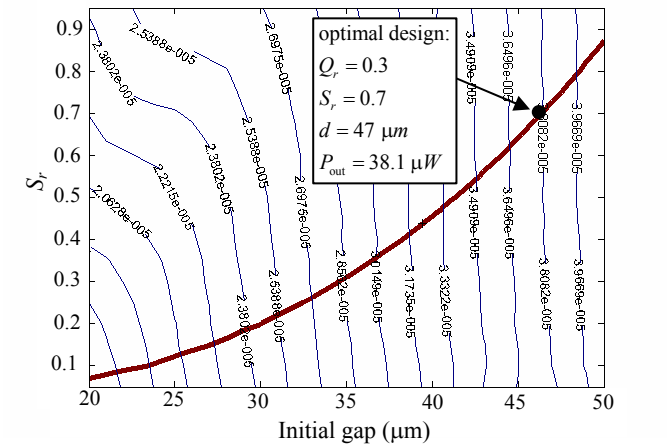

Fig. 7: Output power and voltage contour plot with 4-gm external mass.

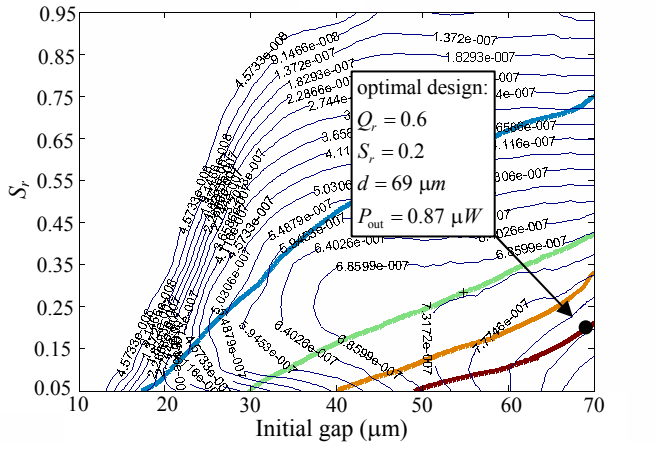

Fig. 8: Output power and voltage contour plot without external mass.

Table 2: Design for max output power below 40 V.

	With 4-gm mass	Without mass
Initial gap d	47 μm	69 μm
Surface ratio S_r	0.7	0.15
Charge ratio Q_r	0.3	0.6
Output power P_{max}	38.1 μW	0.87 μW

4. CONCLUSION

New modeling methodology and optimization parameters were introduced. System dynamics and performance characteristics were found by solving the equations of motion numerically. Optimal design under restricted area and voltage could be determined. It was found that optimized converters could generate significant power only for a limited range of design and operation parameters. Over certain range of these parameters, the converters could not operate stably.

This project was supported in part by the Ministry of National Science Council, Taiwan, R.O.C., under contract no. NSC 98-2220-E-009-040. The authors were grateful to the use of facilities at the National Center for High-performance Computing and the National Nano Device Laboratory, Taiwan, R.O.C..

REFERENCES

[1] S. Roundy and P. K. Wright, 2002, "Micro-electrostatic vibration-to-electricity Converters," *Proc. IMECE 2002,* 39309.

[2] B. C. Yen and J. H. Lang, 2006, "A variable-capacitance vibration-to-electric energy harvester," *IEEE Trans. Circuits and Systems-I,* **53**(2), 288-295.

[3] I. Kuehne, A. Frey, D. Marinkovic, G. Eckstein, and H. Seidel, 2008, "Power MEMS - a capacitive vibration-to-electrical energy converter with built-in voltage," *Sensors and Actuators A,* **142**, 263-269.

[4] D. Hohlfeld, B. Op het Veld, R. J. M. Vullers, and J. de Boeck, 2007, "Coupled-domain modeling of electrostatic energy scavengers and power management circuitry," *Proc. PowerMEMS 2007*, 335-338.

[5] Y. Chiu and F.-G. Tseng, 2008, "A capacitive vibration-to-electricity energy converter with integrated mechanical switches," *J. Micromech. Microeng.,* **18**, 104004.

[6] Y. Chiu, C.-T. Kuo, and Y.-S. Chu, 2007, "MEMS design and fabrication of an electrostatic vibration-to-electricity energy converter," *Microsystem Technologies,* **13**, 1663-1669.

[7] E. Kreyszig, 2005, *Advanced Engineering Mathematics,* 9th ed., Wiley.